Politecnico di Torino

Porto Institutional Repository

[Article] Percolation and Burgers' dynamics in a model of capillary formation

(Article begins on next page)
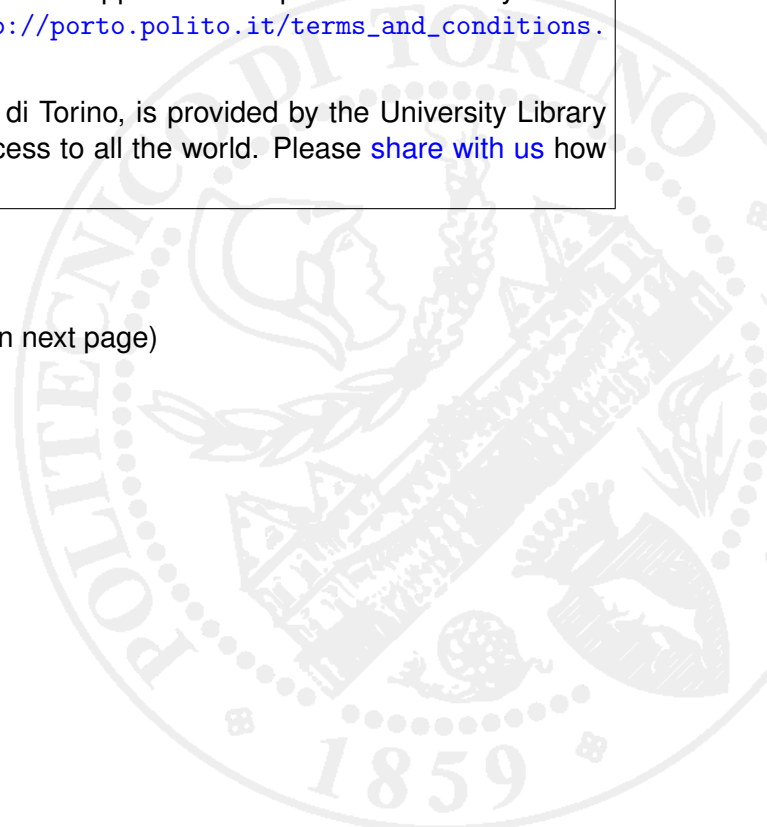
Percolation and Burgers' dynamics in a model of capillary formation

A. Coniglio,[1] A. de Candia,[1] S. Di Talia,[2] and A. Gamba[3]

[1]*Dipartimento di Scienze Fisiche, Università di Napoli "Federico II," 80126 Napoli, Italy*
and Istituto Nazionale di Fisica della Materia, Unità di Napoli, 80126 Napoli, Italy
[2]*International School for Advanced Studies (SISSA-ISAS), 34014 Trieste, Italy*
and Laboratory of Mathematical Physics, The Rockefeller University, New York, New York 10021, USA
[3]*Dipartimento di Matematica, Politecnico di Torino, 10129 Torino, Italy*

Capillary networks are essential in vertebrates to supply tissues with nutrients. Experiments of *in vitro* capillary formation show that cells randomly spread on a gel matrix autonomously organize to form vascular networks. Cells form disconnected networks at low densities and connected ones above a critical density. Above the critical density the network is characterized by a typical mesh size ~ 200 μm, which is approximately constant on a wide range of density values. In this paper we present a full characterization of a recently proposed model which reproduces the main features of the biological system, focusing on its dynamical properties, on the fractal properties of patterns, and on the percolative phase transition. We discuss the relevance of the model in relation with some experiments in living beings and proposed diagnostic methods based on the measurement of the fractal dimension of vascular networks.

PACS number(s): 87.10.+e, 87.17.−d, 64.60.Ak

I. INTRODUCTION

In recent years, biologists have collected many qualitative and quantitative data on the behavior of microscopic components of living beings. We are, however, still far from understanding how these microscopic components interact to build functions which are essential for life. On the other hand, the great success of statistical physics has been the ability to explain the emergence of complex behaviors in physical systems from simplified models of microscopic interactions by a combination of statistical principles and dynamical laws. It seems likely that these tools will turn more and more useful in understanding the behavior of biological systems. One of the areas where this progress can be reasonably expected is the spontaneous formation of complex patterns in living organisms.

The formation of patterns in nature corresponds to various types of symmetry breaking of initially homogeneous systems. Different processes can be reduced to a similar mathematical structure and lead to the formation of patterns whose different realizations share certain common geometrical features. Such patterns often show self-similarity and scaling laws [1] similar to those emerging in the physics of phase transitions [2] and of several kinds of aggregation dynamics [3,4]. For many of these systems it has been shown that scaling laws are directly related to the process which led to the formation of the structure itself [3].

The vascular network [5] is a typical example of natural structure characterized by non trivial scaling laws. In recent years many experimental investigations have been performed on the mechanism of blood vessel formation [6] both in living beings and in *in vitro* experiments. In these experiments, cells are cultured on a gel matrix and their migration and aggregation observed through videomicroscopy. A systematic analysis of such data has led to the discovery of some interesting phenomena and to the proposal of a theoretical model [7] in good agreement with experience [8]. One of the main

observations of Refs. [7,8] is that the system exhibits a percolative transition, forming disconnected networks for low cells densities and connected ones above a critical density ~ 100 cells/mm^2.

The model of Ref. [7] describes the motion of a fluid of randomly seeded independent particles which communicate through emission and absorption of a soluble factor and move toward its concentration gradients. The model allows one to reproduce well both the observed percolative transition and the typical scale of observed vascular networks. While random dispersion of particles at initial time is reminiscent of standard percolative models, here an important role is played by migration and dynamical aggregation of particles. The model appears thus as a possibly new and physically interesting representative in the class of percolation models.

In this paper we present a complete characterization and discussion of the model focusing on the process of aggregation, on percolative critical behavior, and on fractal structures observed at small and large scales. The dynamics, described by a Burgers-like equation, is discussed in the framework of the hydrodynamics of a fluid of noninteracting particles focusing on differences and analogies with the original Burgers' system. The percolative critical behavior and the geometry of patterns are studied using scaling relations, computing critical indices and the fractal dimension through extensive numerical simulations and analysis of the experimental data.

We verify the agreement of numerical simulations with experimental observations, as discussed in Ref. [7], extending the analysis to cluster distributions. The numerical results show that the transition is in the universality class of random percolation, even in the presence of migration and dynamical aggregation, which changes the pattern geometry at small scales as shown by the calculation of the fractal dimension at any scale.

The paper is organized as follows. Section II summarizes some background knowledge on the biological problem of vascular network formation and the main experimental observations of Ref. [8]. Section III is a short review of results in the hydrodynamics of noninteracting particles. In Sec. IV a full characterization of the model that appeared in Ref. [7] is presented, while in Sec. V the main results on the critical behavior and the fractal structures of model and experiments are presented. In the conclusions we discuss the relevance of our results in relation to some recent *in vivo* experiments and diagnostic methods based on the measurement of the fractal dimension of vascular networks which have been proposed in the literature [9].

II. BIOLOGICAL FRAMEWORK AND EXPERIMENTAL OBSERVATIONS

To supply tissues with nutrients in an optimal way, vertebrates have developed a hierarchical vascular system which terminates in a network of size-invariant units, i.e., capillaries. Capillary networks characterized by intercapillary distances ranging from 50 to 300 μm are essential for optimal metabolic exchange [10].

Capillaries are made of endothelial cells. Their growth is essentially driven by two processes: vasculogenesis and angiogenesis [6]. Vasculogenesis consists of local differentiation of some precursor cells to endothelial ones that assemble into a vascular network by directed migration and cohesion. Angiogenesis is, essentially, characterized by sprouting of an immature structure and remodeling.

In the early embryonic life, capillaries are formed by vasculogenesis which brings the formation of a primitive vascular network. Angiogenesis integrates vasculogenesis forming new capillaries from existing ones. The growth of blood vessels in the developing organs is basically the result of an invasion process by capillaries into the early organs' structures. It has been proven and accepted that during tumorigenesis angiogenesis is essential to provide the requisite nutritional supply to growing tumors (for a review see Ref. [6]). Carmeliet in Ref. [6] speculates that recent findings of mosaic tumor vessels and vasculogenic tumor cells "may have considerable consequences for antiangiogenic tumor therapy".

Experiments have shown that endothelial cells cultured on Matrigel, a surface which favors cell motility and has biochemical characteristics similar to living tissues, self-assemble to form geometric tubular networks, which are almost identical to capillary vascular beds observed in living beings [11].

The process of formation of a vascular network starting from randomly seeded cells can be accurately tracked by videomicroscopy [8] and it is observed to proceed along three main stages (see Fig. 1): (i) migration and early network formation, (ii) network remodeling, and (iii) differentiation in tubular structures. During the first phase, which is the most important for the geometrical properties of the structures, cells migrate over distances which are an order of magnitude larger than their radius and aggregate when they get in touch with one of their neighbors. In a time of the
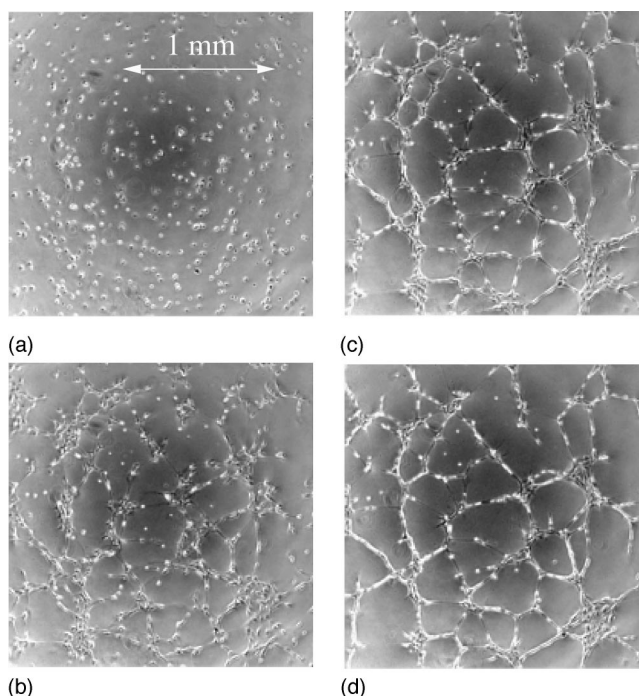

FIG. 1. Experimental pictures of the dynamical process of vascular network formation obtained starting with an initial cell density of 200 cells/mm^2. (a) $t=0h$; (b) $t=3h$; (c) $t=6h$; (d) $t=9h$. The side of the box is 2 mm. Observe that bright spots and darker edges appearing in the pictures are an artifact of phase-contrast microscopy but all correspond to the same kind of cellular matter. On the other hand, the Matrigel background is easily recognizable from the homogeneous gray color.

order of 10 h they form a continuous multicellular network which can be described as a collection of nodes connected by chords. The mean chord length is approximately independent on the initial cell density $\bar{n}$, with an average value $\bar{\ell} \simeq 200$ μm for $\bar{n}$ ranging from 100 to 200 cells/mm^2. By varying the initial cell density one observes the clear signs of a percolative transition (Fig. 2). Below a critical value $n_c \sim 100$ cells/mm^2 groups of disconnected structures are formed [Fig. 2(a)]. For $\bar{n} \geqslant n_c$ a single connected network is instead visible [Figs. 2(b) and 2(c)]. For higher values of $\bar{n}$ one observes a sort of "Swiss-cheese" pattern [Fig. 2(d)].

An accurate statistics of individual cells trajectories has been presented in Ref. [8], showing that in the first phase cell motion has marked persistence in the initial direction, pointing toward zones of higher concentrations of cells. This indicates that cells communicate among them through the emission of soluble chemical factors that diffuse and degrade in the surrounding medium, and suggests that they move toward the gradients of this chemical field. The statistics of individual cells trajectories in a simulated chemotactic field strongly support the model [8]. Cells behave like not-directly interacting particles, the interaction being mediated by the release of chemotactic factors.

It is interesting to observe here that direct evidence of the cell-cell interacting mechanism essential for pattern formation is very difficult to obtain experimentally. A quantitative model based on microscopic assumptions, however, allows
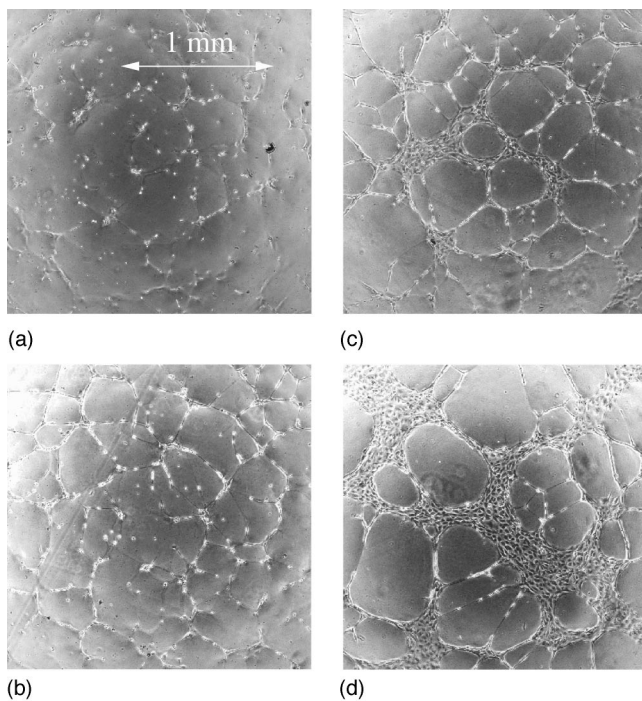
(a) (c)

(b) (d)

FIG. 2. Experimental pictures of vascular structures obtained starting from four different values of the initial cell density. (a) 50 cells/mm^2; (b) 100 cells/mm^2; (c) 200 cells/mm^2; (d) 400 cells/mm^2. The side of the box is 2 mm.

to obtain important indirect evidence on the molecular mechanism, making clear predictions of the macroscopic behavior that can be easily verified experimentally.

III. BURGERS' EQUATION

The hydrodynamics of noninteracting particles has been studied in many different contexts, e.g., in astrophysics, to describe the emergence of structures from an initial uniform density [12], and in condensed matter to describe molecular surface growth and granular materials [13,14]. Among such systems, an interesting case is that of weakly interacting sticky matter. In the early stages of dynamics, each particle moves with a constant velocity, given by a random statistical distribution. This motion gives rise to intersection of trajectories and formation of shock waves. After the birth of these local singularities (caustics) regions of high density grow and form a peculiar structure. The main feature of this structure is the existence of comparatively thin layers and filaments of high density that separate large regions of low density. This is an intermediate state: if the initial velocity field satisfies natural statistical properties, then the final state will be a Maxwellian thermal equilibrium distribution with normal coarse-grained density fluctuations. The behavior of these systems can be described in detail by Burgers' equation [15]:

$$\frac{\partial \mathbf{v}}{\partial t} + \mathbf{v} \cdot \boldsymbol{\nabla} \mathbf{v} = \nu \nabla^2 \mathbf{v}, \tag{1}$$

coupled with the mass-conservation law:

$$\frac{\partial n}{\partial t} + \boldsymbol{\nabla} \cdot (n\mathbf{v}) = 0. \tag{2}$$

These equations are a well established paradigm in the theory of self-organized aggregation and pattern formation and have been utilized to describe the emergence of structured patterns in many different physical settings [12,13].

Assuming that the initial velocity is potential, $\mathbf{v}_0(\mathbf{a}) = -\boldsymbol{\nabla} \psi_0(\mathbf{a})$, this condition yields also for later times and the potential ψ obeys to the Kardar, Parisi, and Zhang (KPZ) equation [13]:

$$\frac{\partial \psi}{\partial t} = \frac{1}{2}(\boldsymbol{\nabla} \psi)^2 + \nu \nabla^2 \psi.$$

As observed by Hopf [16] and Cole [17], the change of variable $\psi = 2\nu \ln \theta$ changes the nonlinear KPZ equation into a heat equation, thereby leading to the explicit solution, if there are no boundaries:

$$\psi(\mathbf{r},t) = 2\nu \ln \frac{1}{(4\pi\nu t)^d} \int_{R^d} \exp\left[\frac{1}{2\nu}\left(\psi_0(\mathbf{a}) - \frac{|\mathbf{r}-\mathbf{a}|^2}{2t}\right)\right] d^d a. \tag{3}$$

In the $\nu \to 0$ limit (which coincides with the case of noninteracting particles) using the steepest descent method one obtains that

$$\psi(\mathbf{r},t) = \max_{\mathbf{a}}\left(\psi_0(\mathbf{a}) - \frac{|\mathbf{r}-\mathbf{a}|^2}{2t}\right). \tag{4}$$

In the points where $\psi_0(\mathbf{a})$ is differentiable one easily obtains that the map between initial coordinates (Lagrangian coordinates) and actual ones (Eulerian) is given by the relation

$$\mathbf{r} = \mathbf{a} + \mathbf{v}_0(\mathbf{a})t. \tag{5}$$

Formal use of this relation apparently predicts overshooting, i.e., in some regions one point $\mathbf{r}$ corresponds to more points with different $\mathbf{a}$. Actually only the point which maximizes ψ must be taken. The other points must have generated a δ function concentration of matter at a previous stage. This means that the relation (5) gives the correct behavior only when it is invertible. It can be easily shown that the first time when the map becomes multivalued is [18]

$$t_* = \frac{1}{\max_{\mathbf{a}}[\lambda_i(\mathbf{a})]}, \tag{6}$$

where λ_i are the eigenvalues of the Hessian matrix $\partial^2 \psi_0 / \partial a_i \partial a_j$ [18].

A nonvanishing value of ν, no matter how small, prevents the interpenetration of particles in the sense that on scales of order $\delta \sim \nu\tau/l$, where τ and l are typical time and length scales, the Laplacian term becomes important and dissipation prevents the faster particles from overcoming the slow ones. This has the physical effect that once a fast particle catches up to a slow one they stick together and continue their motion as a whole.
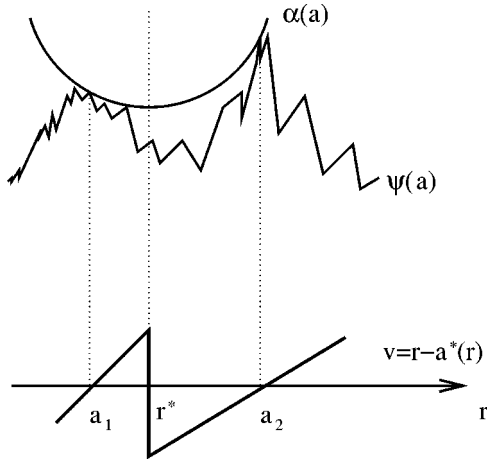
FIG. 3. Construction of the solution with the parabola method for a given realization of the initial potential $\psi_0(a)$. The parabola $\alpha(a)$ centered in a Eulerian point r^* touches the potential in two points a_1, a_2. This corresponds to the formation of a shock in the velocity field at the Eulerian point r^*.

The arbitrary parameter ν can be interpreted as viscosity, even if the way it enters into the equation implies a model description of viscosity rather than a physical one.

The velocity field can be recovered from the relation

$$\mathbf{v}(\mathbf{r},t) = \frac{\mathbf{r} - \mathbf{a}^*(\mathbf{r},t)}{t} \tag{7}$$

where $\mathbf{a}^*$ is the point which verifies relation (4).

Equation (4) is the basis of much work on Burgers' equation. It gives a nice geometrical construction of the solution starting with the initial conditions $\psi_0(\mathbf{a})$. We recall the argument in the one-dimensional case, the extension to the higher dimensional case being straightforward.

Evaluating the expression in the right-hand side of Eq. (4) is equivalent to finding points where the distance between the parabola $\alpha(r,a,t) = |r-a|^2/2t$ and the initial potential $\psi_0(a)$ is minimum, or points where the parabola $\alpha(r,a,t) + H$, where H is a constant, touches for the first time the initial potential $\psi_0(a)$. The behavior of these extreme points is regulated by the curvature of the parabola, i.e., $1/t$, and that of the initial potential $\sim v_0/l_0$, where l_0 is a typical length scale of the initial potential. For times such that $t \ll l_0/v_0$ the parabola has a large curvature and the point where Eq. (4) is satisfied is unique. During the course of time the curvature of the parabola diminishes and finally there will be a point where two Lagrangian points will correspond to the same Eulerian one. This corresponds to the formation of a shock. From this construction it is easy to understand that the velocity field will tend to a sawtooth behavior [Fig. 3].

To understand the behavior of the density field, one can use the mass-conservation law [18]. This implies that at regular points the density is given by

$$n(\mathbf{r},t) = \frac{n_0(\mathbf{a})}{J(\mathbf{a},t)}, \tag{8}$$

where J is the Jacobian of the Lagrangian map. Since the Jacobian is [up to a factor $(-1)^d$] equal to the Hessian of the Lagrangian potential $\varphi(\mathbf{a},t) = t\psi_0(\mathbf{a}) - a^2/2$ it follows that large densities are typically obtained near points where the Hessian vanishes [12].

Many analytic and numerical techniques have been developed to understand the properties of systems described by higher dimensional Burgers' dynamics (for a review see Ref. [19]). It has been shown that they develop in a finite time shock waves corresponding to faster particles overcoming slower ones, just as in the one-dimensional case. One observes the formation of a networklike pattern of shock waves, which after some time can be well described as groups of nodes connected by chords [20]. The geometry of these patterns is linked to the properties of the initial conditions and for typical initial conditions (Gaussian density fluctuations with a power-law spectrum, which implies that also the initial velocity is Gaussian with a power-law spectrum) does not show any typical length scale. A power-law scaling at small masses (compared to the average mass) is observed in the behavior of the cumulated mass function, defined as the number of shock intervals having a length greater than the mass. For large masses, a power-law for the logarithm of the cumulated mass function is observed. Some of these results can be derived analytically for the one-dimensional case [21].

IV. THE MODEL

The first phase of the dynamical process of *in vitro* capillary formation described in Sec. II has many similarities with the process of pattern formation in Burgers' equation. This point of view is supported by the statistics of individual cells trajectories [8], showing that the kinematics of cells is well described by a set of not directly interacting particles, approximately moving along straight lines. With respect to the original Burgers model however one has an additional effect, since cell velocities are believed to be formed as a consequence of the detection by the cell themselves of spatial gradients of a chemotactic factor.

A model based on such assumptions has been proposed [7], which turns out to be in strikingly good agreement with experimental observations. The model describes the cell population as a continuous distribution of density n and velocity $\mathbf{v}$; it also assumes the presence of a concentration field c of soluble factors. Cells are modeled as a fluid of not directly interacting particles accelerated by gradients of soluble factors, which are supposed to be released by cells, diffuse, and degrade in finite time, as suggested by experimental observations. These assumptions give rise to the following equations:

$$\frac{\partial n}{\partial t} + \boldsymbol{\nabla} \cdot (n\mathbf{v}) = 0, \tag{9a}$$

$$\frac{\partial \mathbf{v}}{\partial t} + \mathbf{v} \cdot \boldsymbol{\nabla} \mathbf{v} = \mu \boldsymbol{\nabla} c, \tag{9b}$$

$$\frac{\partial c}{\partial t} = D\boldsymbol{\nabla}^2 c + \alpha n - \tau^{-1}c, \tag{9c}$$

where D, α, τ are respectively, the diffusion coefficient, the rate of release, and the characteristic degradation time of soluble mediators, and μ measures the strength of cell re-

sponse. Initial conditions are given in the form of a set of randomly distributed bell-shaped bumps having width of the order of the average cell radius a and null velocities.

The physical content of the model is the following. Equation (9a) expresses the conservation of the number of cells. At low densities, Eq. (9b) is an in viscid Burgers' equation for the velocity field **v** [15], coupled to the standard reaction-diffusion equation, (9c). In Burgers' equation matter in the earlier stages of its evolution is described as a fluid of free, noninteracting particles. The free particle fluid dynamics has the effect of strongly amplifying even small inhomogeneities in the initial data. After a characteristic time, faster particles catch up to the slower ones and form a network of shock waves, which in two dimensions are strikingly similar to capillarylike networks.

Equation (9b), as explained in Sec. III, has the characteristics that solutions can become multivalued, corresponding to faster particles overcoming the slower ones. This is usually prevented by adding in the right-hand side of Eq. (9b) a regularizing term $\nu \nabla^2 \mathbf{v}$. Instead of viscosity, one can introduce a phenomenological, density dependent pressure term $-\nabla \phi(n)$, in the right-hand side of Eq. (9b), with $\phi(n)$ zero for low densities and rapidly increasing for densities above some threshold, in order to describe the fact that cells do not interpenetrate.

Fourier analysis of Eq. (9c) in the fast diffusion approximation ($\partial c/\partial t = 0$) suggests that starting from the above mentioned initial conditions, Eq. (9) should develop network patterns characterized by a typical length scale $r_0 = \sqrt{D\tau}$, which is the effective range of the interaction mediated by soluble factors. As a matter of fact, Fourier components c_k are related to the Fourier components of the density field n_k by the relation $c_k = \alpha \tau n_k / D\tau k^2 + 1$. This means that in Eq. (9b) wavelengths of the field n of order r_0 are amplified, while wavelengths $\lambda \gg r_0$ or $\lambda \ll r_0$ are suppressed.

Initial conditions introduce in the problem a typical length scale given by the average cell-cell distance $L/\sqrt{N}$, where L is the system size and N the particle number. The dynamics, filtering wavelengths, rearranges matter and forms a network characterized by the typical length scale r_0. Numerical simulations confirm this theoretical prediction.

It is interesting to check the compatibility of the theoretical prediction with physical data. From available experimental results [22] it is known that the order of magnitude of the diffusion coefficient for major angiogenic growth factors is $D = 10^{-7}$ cm^2 s^{-1}. In the experimental conditions that were considered the half time of soluble factors is 64 ± 7 min [8]. This gives $r_0 \sim 200$ μm, a value in good agreement with experimental observations.

The coupling with Eq. (9c), then, introduces in the problem the natural length scale r_0. This suggests a simple theoretical mechanism accounting for the experimentally observed characteristic size of capillary structures.

In real space, the scenario is as follows. Initially, nonzero velocities are built up by the chemoattractive term due to the presence of random inhomogeneities in the density distribution. Then, Burgers' dynamics amplifies the inhomogeneities and forms a capillarylike network. In the fast diffusion approximation, density inhomogeneities are instantaneously translated in a landscape of concentration of soluble factors

where details of scales $\lesssim r_0$ are averaged out by the action of the nonlocal operator $\mu \nabla [r_0^2 - (\nabla^2)^{-1}]$. Particles move toward the crests of the landscape, which are separated by valleys of width $\sim r_0$. Burgers' dynamics sharpens the crests and empties the valleys in the concentration landscape, eventually producing a network structure characterized by a length scale of order r_0. In this way, the model provides a most direct link between the structure dimensions and the range of intercellular interaction.

All these theoretical insights are confirmed by numerical simulations. The numerical simulations were performed with periodic boundary conditions, using a finite volume method [23]. We used the experimental values for D and τ, while the unknown parameters μ, α were set to 1 (which amounts to an appropriate rescaling of time and the concentration field c). Initial conditions were given by throwing the same number of cells as in the biological experiments in random positions inside the box, with zero velocities and zero concentration of the soluble factor, with a single cell given initially by a Gaussian bump of width σ of the order of the average cell radius ($a \simeq 30$ μm) and unitary weight in the integrated cell density field n. Starting from these conditions, Eq. (9) were numerically integrated. The simulation was stopped when the vascular network was formed or a stationary state was reached.

In Figs. 4–6 the results of four simulations at different time steps and for different values of the density and of the interaction range are shown. Black areas represent regions filled with cells, that is, regions where the density exceeds a given threshold; white areas represent the underlying substrate. The threshold was chosen to coincide with the close-packing density $\sim 1/(2\pi\sigma^2)$. The model reproduces quite well the dynamical process of pattern formation and typical structure of the vascular network, with chords of length $\bar{\ell} \simeq 200$ μm for a wide range of cell densities. As in the case of experimental data, a percolative transition is observed at a critical cell density n_c.

V. ANALYSIS OF PERCOLATIVE PHASE TRANSITION

A. General framework

The purely geometric problem of percolation represents one of the simplest phase transition occurring in nature. Many percolative models show a second-order phase transition in correspondence to a critical value n_c, i.e., the probability Π of observing an infinite cluster is 0 for $\bar{n} < n_c$ and 1 for $\bar{n} > n_c$ [24]

It is natural to chose as order parameter the probability P that a randomly chosen site belongs to an infinite cluster, while the analog of magnetic susceptivity in a ferromagnetic transition is the average cluster size

$$S = \frac{\sum_s N_s s^2}{\sum_s N_s s},$$

where N_s is the number of clusters of size s, excluding from the sum the infinite cluster. S is the average size (number of
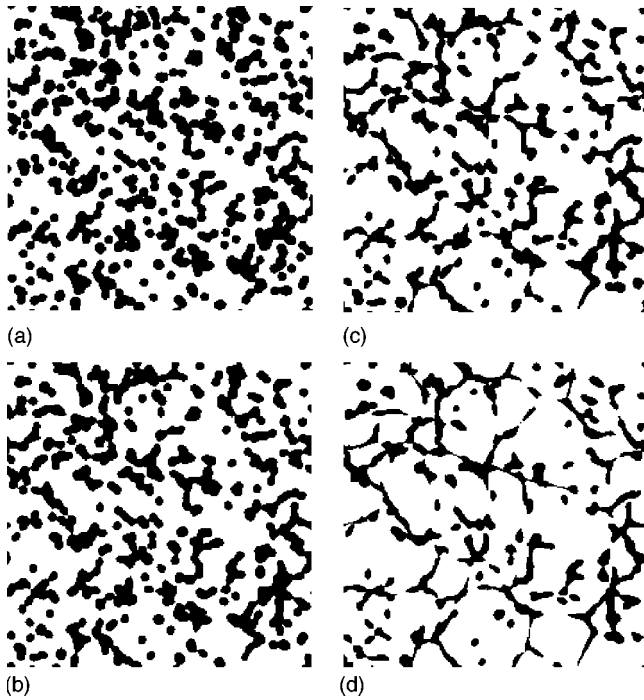
FIG. 4. Numerical simulations of the pattern formation process at different times obtained starting from initial cell density 100 cells/mm^2. (a) $t=0$ h (b) $t=3$ h (c) $t=6$ h; (d) $t=9$ h. The side of the box is 2 mm. In the simulated network structures one recognizes sometimes blobs connected by narrow bridges. The blobs are what remains of isolated cells or small cell aggregates after chemotactic aggregation and their size is of order r_0. The width of the bridges is probably a nonuniversal quantity depending on several factors, including the particular form of the pressure term $\phi(n)$. A more detailed physical modeling could probably allow to fit the experimentally observed width distribution.

sites) to which a randomly chosen occupied site in the lattice belongs.

The correlation (or connectivity) function $c(r)$ is defined as the probability that two randomly chosen sites at distance r are occupied on the same cluster and the correlation (or connectivity) length as

$$\xi^2 = \frac{\sum r^2 c(r)}{\sum c(r)},$$

where the sum is performed over sites.

In a neighborhood of the critical point the following critical behaviors are observed:

$$\Pi = \theta(\bar{n} - n_c), \tag{10a}$$

$$P \sim (\bar{n} - n_c)^\beta \quad \text{for} \quad \bar{n} \geqslant n_c, \tag{10b}$$

$$S \sim |\bar{n} - n_c|^{-\gamma}, \tag{10c}$$

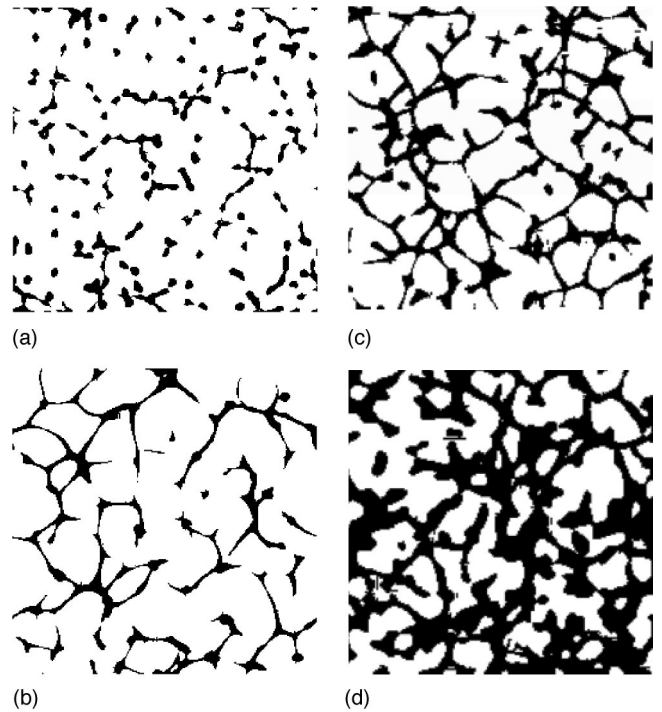$$N_s \sim s^{-\tau} \quad \text{for} \quad \bar{n} = n_c, \tag{10d}$$

FIG. 5. Numerical simulations obtained starting from four different values of the initial cell density. (a) 50 cells/mm^2; (b) 100 cells/mm^2; (c) 200 cells/mm^2; (d) 400 cells/mm^2. The side of the box is 2 mm.

$$c(r) \sim r^{-\eta} \quad \text{for} \quad \bar{n} = n_c, \tag{10e}$$

$$\xi \sim |\bar{n} - n_c|^{-\nu}, \tag{10f}$$

where β, γ, τ, η, ν are the critical exponents and θ the step function.

On systems of finite size L, the first three quantities obey the following finite size scaling relations:

$$\Pi(\bar{n},L) \sim \hat{\Pi}[(\bar{n} - n_c)L^{1/\nu}], \tag{11a}$$

$$P(\bar{n},L) \sim L^{-\beta/\nu}\hat{P}[(\bar{n} - n_c)L^{1/\nu}], \tag{11b}$$

$$S(\bar{n},L) \sim L^{\gamma/\nu}\hat{S}[(\bar{n} - n_c)L^{1/\nu}]. \tag{11c}$$

Another quantity of interest is the density function $\rho(r)$ of the percolating cluster for various r. This function is defined as the mean density of sites belonging to the percolating cluster, enclosed in a circle of radius r centered at one site belonging to the cluster, and averaged over different centering sites and different realizations of the system. For a fractal object with fractal dimension D, this should scale as $\rho(r) \sim r^{D-d}$. This behavior is expected for percolating clusters at the critical point.

It is well known that only two critical exponents are independent, since critical exponents are constrained by scaling laws [2].
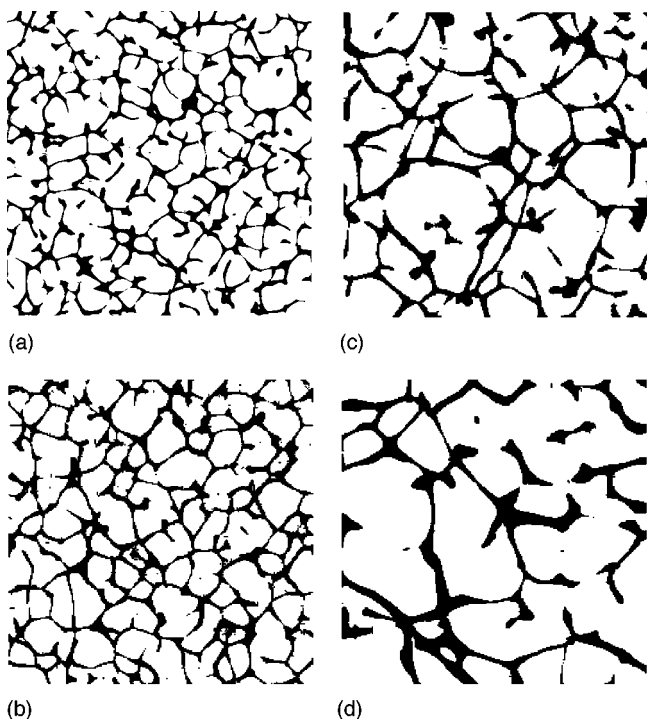
FIG. 6. Numerical simulations obtained with different values of the interaction range r_0. (a) $r_0 = 100 \, \mu m$; (b) $r_0 = 200 \, \mu m$; (c) $r_0 = 300 \, \mu m$; (d) $r_0 = 400 \, \mu m$. The side of the box is 2 mm.

B. Numerical computation of critical indices

To characterize the observed percolative phase transition, extensive numerical simulations of system (9) were performed on a Beowulf network of 14 knots using lattice sizes $L = 1, 2, 4,$ and 8 mm, with different values of the initial density $\bar{n}$ (see, e.g., Fig. 5).

For each point 100 to 200 realizations of the system were computed, depending on the proximity to the critical point.

In order to study percolation properties the square domain was partitioned in little square boxes of size 2^{-6} mm, forming the sites of a square lattice; the system (9) was solved using a finite volume method on this lattice and each site set as filled if the mean cell density inside the corresponding little box was larger than the threshold $1/2\pi\sigma^2$, empty otherwise [25]. We then identified clusters of nearest neighbor filled sites.

We thus mapped the continuous density n to a set of occupied and empty sites. Using a Hoshen-Kopelman algorithm [26] we then measured the following for each set of realizations.

(1) The percolation probability Π.
(2) The fraction of sites belonging to the largest cluster, which for an infinitely large system gives the percolation strength P.
(3) The mean cluster size S.
(4) The cluster distribution function N_s.

Using relation (11a), we estimate the position of the critical point n_c from the intersection of graphs of $\Pi = \Pi(\bar{n}, L)$ (Fig. 7). For the chosen threshold $1/(2\pi\sigma^{-2})$, the estimated value is $n_c = 94 \pm 1$ cell/mm^2.
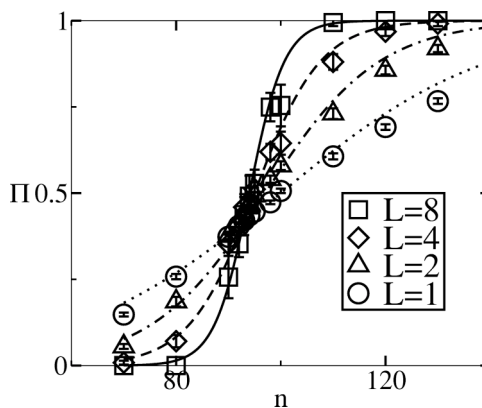

FIG. 7. Percolation probability as a function of $\bar{n}$ for different sizes L. The curves have fitted to the numerically computed points and are intended as a guide to the eye.

Then, we find ν plotting $\Pi(\bar{n}, L)$ as a function of $(\bar{n} - n_c)L^{1/\nu}$, where n_c is held to the value previously computed and looking for the value of the exponent which allows the best data collapsing according to relation (11a) (Fig. 8). We obtain $\nu = 1.33 \pm 0.08$.

Knowing ν and n_c, we estimate β/ν and γ/ν by looking for the data collapse of $L^{\beta/\nu}P(\bar{n}, L)$ and $L^{-\gamma/\nu}S(\bar{n}, L)$ as a function of $(\bar{n} - n_c)L^{1/\nu}$, according to the relations (11b) and (11c) (see Figs. 9 and 10). We obtain $\beta/\nu = 0.11 \pm 0.01$ and $\gamma/\nu = 1.83 \pm 0.05$. The errors on computed values of indices are estimated looking for the range of values that gives an acceptable data collapse.

By the cluster distribution function behavior at critical point we estimate the critical exponent τ using the relation (10d). We obtain $\tau = 2.0 \pm 0.1$ (see Fig. 11).

Computing $\rho(r)$ at the critical point we measure D, obtaining $D = 1.87 \pm 0.03$ (see Fig. 12); the error is principally due to the uncertainty in the determination of n_c.

Numerical data suggest that the phase transition be second order. The values found for ν, γ/ν, β/ν, τ, and D with the corresponding errors are compatible with the scaling laws.

We verified that while n_c is sensitive to the choice of the threshold in a neighborhood of the natural value $1/(2\pi\sigma^2)$,
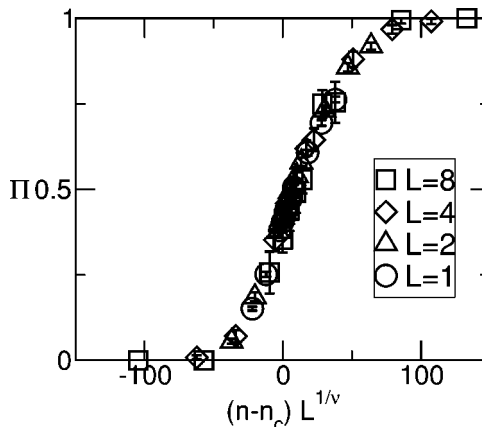

FIG. 8. Collapsing of the data shown in Fig. 7 using Eq. (11a) with $\nu = 1.33$.
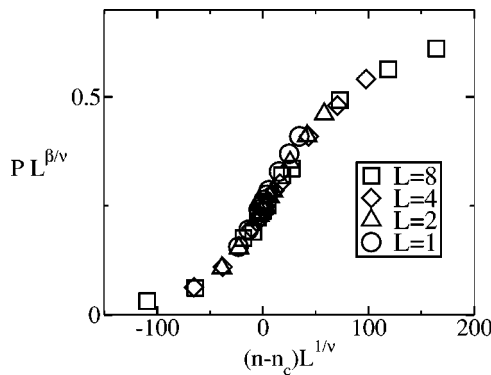
FIG. 9. Order parameter data with different values of the size L collapsed using Eq. (11b) with $\nu=1.33$, $\beta/\nu=0.11$.

FIG. 11. Cluster distribution function N_s from numerical simulation as a function of s for percolating cluster at critical point.

the critical exponents do not depend on it. This is what one expects for universality of critical models.

A comparison with the critical indices of random percolation [24] gives numerical evidence that the phase transition falls in the universality class of random percolation (see Table I), that is, when the sites of the lattice are uncorrelated and each one occupied with the same probability. As critical indices are linked to the large-scale structure of the percolating cluster, this means that, on such a large scale, the structure of the vascular network is mainly determined by initial random positioning of the cells, and is not altered by the dynamical process of migration and aggregation. This is what one expects because the interaction among cells is mediated by a finite-range interaction. So at scales $\gg r_0$ the structure of the percolating cluster is determined by the coalescence of aggregates of sizes of order $\sim r_0$.

C. Small scales behavior

The critical exponents listed before give information about the large-scale behavior of the system. On the other hand, in smaller distances clusters are quite different from the ones of random percolation. In order to get some understanding on smaller scales geometry we measured the density function $\rho(r)$ at $\bar{n}=n_c$ of the percolating cluster (defined as the largest cluster) for various r.

This function clearly shows that two regimes are present. At scales $r \lesssim r_c=0.77\pm0.08$ mm the behavior of the system

is different from that of random percolation and a different fractal dimension $D=1.50\pm0.02$ is observed, while at larger scales one finds again the behavior of random percolation. As explained in the preceding section the large-scale behavior of the system is essentially regulated by initial random conditions. The fractal dimension at small scales is related to the dynamical process of migration and aggregation.

The exponent τ is directly related to the fractal dimension by the relation $\tau=1+d/D$, so it would be interesting to check if a crossover behavior could be observed also in this function or not (which is not obvious). Unfortunately, our data are not enough to see if this crossover is present or not.

A class of fractal growth models, which shows a value for the fractal dimension $D\sim1.5$ (similar to the one observed at small scales), is cluster-cluster aggregation [3]. In cluster-cluster aggregation models, it is assumed that starting with random initial conditions particles can diffuse according to some rule and stick with a certain probability when they get in touch. Clusters formed in this process then diffuse and the process ends with the presence of a small number of large clusters.

The framework of cluster-cluster aggregation seems to be similar in some way to the situation described in this paper. The main difference is in the fact that cluster-cluster aggregation models consider random (diffusive) motions instead of the directed motions considered in this paper.
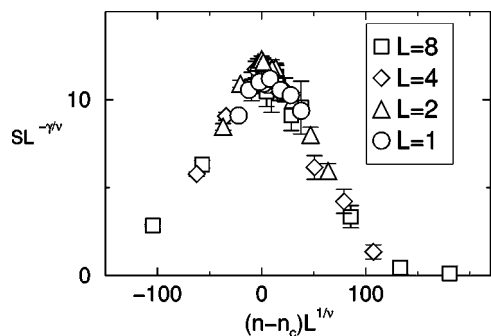

FIG. 10. Mean cluster size data with different values of the size L collapsed using Eq. (11c) with $\nu=1.33$, and $\gamma/\nu=1.83$.
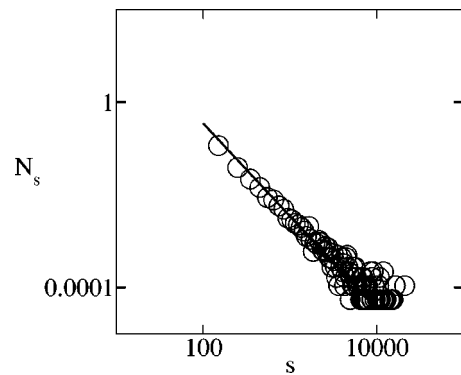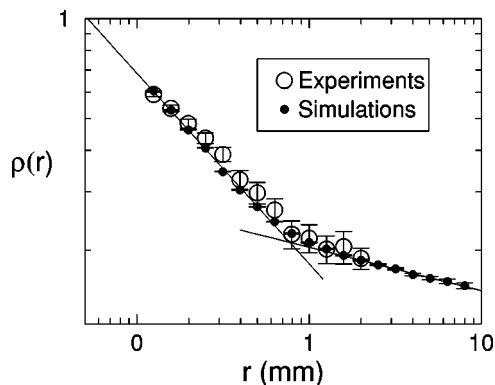

FIG. 12. Density of the percolating cluster $\rho(r)$ as a function of radius for numerical and experimental data.

TABLE I. Critical indices measured on the numerical model and on experimental data, and compared with the exact values of random percolation.

Critical index	Model	Experiments	Random percolation
ν	1.33 ± 0.08	Not measured	1.333
γ/ν	1.83 ± 0.05	1.78 ± 0.12	1.792
β/ν	0.11 ± 0.01	Not measured	0.104
τ	2.0 ± 0.1	2.0 ± 0.3	2.055
D	1.87 ± 0.03	1.85 ± 0.10	1.896

D. Analysis of experimental data

In order to verify the agreement of numerical calculations and experimental data we repeated the measures described above on experimental data kindly provided by Bussolino and Serini at IRCC (Candiolo, Turin). The data consist of a set of 28 digital photographs (with a resolution of 1024^2 pixels) of mature structures obtained starting from initial densities of $50, 75, 100, \ldots, 200$ cells/mm^2. The photographs are the results of two experimental sessions, each performed in duplicate, so that four photographs are available for each density value.

An analysis of these data was already presented in Ref. [7]. The data show the presence of a percolative transition at $n_c \sim 125$ cells/mm^2, and are compatible with the values for γ/ν and τ obtained from numerical simulations (Figs. 13 and 14). The available data are not enough to obtain ν and β/ν with a reasonable precision [7]. The density $\rho(r)$ of the percolating cluster as a function of the radius was also measured, showing perfect agreement with the numerical computations (see Fig. 12). We obtain $D = 1.85 \pm 0.10$ for the fractal dimension, while at small scales this exponent becomes $D = 1.48 \pm 0.05$. The crossover point is practically identical to the numerically computed one.

We plan to repeat the measures on a larger set of experimental data as soon as they become available.

VI. CONCLUSIONS

We have presented an extensive discussion of the dynamical properties of the model proposed in Ref. [7] and analyzed
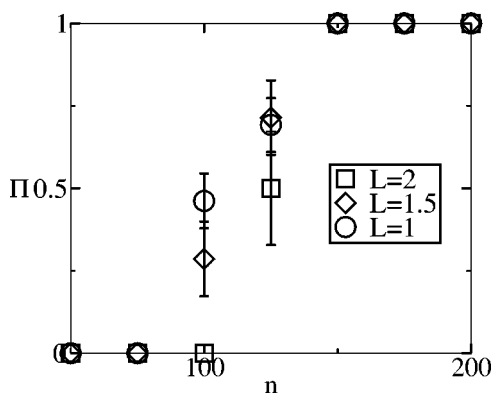
FIG. 13. Percolation probability measured from experimental pictures as a function of $\bar{n}$ for different L.
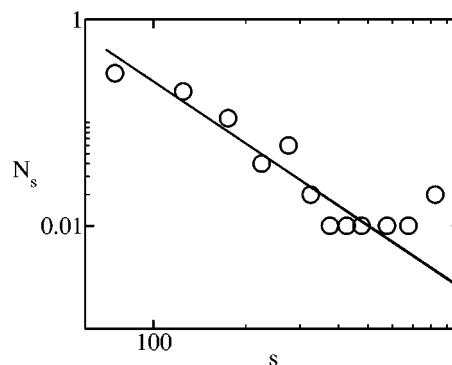
FIG. 14. Cluster distribution function N_s from experimental data as a function of s for the percolating cluster at the critical point.

numerical results on the percolative critical behavior and fractal structures in connection with experimental data. Critical indices of the phase transition and fractal dimension of numerically computed patterns are in good agreement with experimental results, although with the limitations due to the small number of experimental pictures available. The phase transition appears to be second order, at least to the accuracy allowed by the limitations in size which are intrinsic to our numerical experiments. Comparison of critical indices suggests that the phase transition falls in the universality class of random percolation, even in presence of migration and dynamical aggregation.

This is expected because the dynamical mechanism of migration and aggregation is short range, so that critical behavior is regulated by initial random conditions. The small-scale behavior is different, being strictly linked to the dynamical mechanism of migration and aggregation, as suggested in Ref. [7].

We have also shown that endothelial cells endowed with a specific gene profile act according to simple mathematical laws, which ultimately govern vascular network assembly and geometry. This suggests that capillary structures themselves may have evolved as a consequence of these fundamental abilities of specific cell populations, such as motility and adhesion, in much the same way as it happened with nonliving matter, on an enormously different length scale, when the large-scale structure of the Universe formed from a presumably initial uniform background.

The model appears to be quite successful in describing *in vitro* experiments, where all the parameters are under control and one can easily tune the cell density.

Our numerical computation could in principle present some practical implication. Normal tissue function depends on adequate supply of oxygen through blood vessels. Understanding the mechanisms of formation of blood vessels has become a principal objective of medical research, because it would offer the possibility of testing medical treatments *in silicio*. One can think that the dynamical model described in this paper can be utilized in future to design properly vascularized artificial tissues by controlling the vascularization process through appropriate signaling patterns.

Some recent *in vivo* results [27] seem to suggest that a mechanism similar to that studied here could be essential also in some *in vivo* situations. It is known that the soluble

growth factor VEGF-A exists in several isoforms characterized by different molecular weights and diffusivities. In Ref. [27] it was shown that mouse embryos engineered to express solely an isoform of VEGF-A characterized by larger diffusivity exhibit a specific vessel patterning defect that results in the creation of capillary networks with larger mesh size. Figures 2(d)–2(f) of Ref. [27] are strikingly reminiscent of our simulations of model (9) with varying interaction range (Figs. 6). Although the interpretation of the *in vivo* results of Ref. [27] leaves several open questions which deserve further investigations [8], the data appears to be coherent with the general scheme described in this paper.

It was suggested [9] that different kinds of vascular networks, as, e.g., vascular networks grown in tumors or in normal tissues, can be discriminated by measuring their fractal dimension D. In experiments performed on mouse skin vascularization, in particular, the dimension of normal capillaries of sizes ranging from 50 to 900 μm appears to be very close to 2. However, it is pointed out by the authors that such space-filling structures are difficult to explain by the generally accepted paradigm of diffusion limited aggregation, that would provide $D \sim 1.70 \pm 0.06$ [3].

It seems likely that while angiogenesis can be described by diffusion limited aggregation, vasculogenesis, where random differentiation of a fraction of endothelial cells is followed by migration and aggregation, is instead closer to the kind of percolation problem that was studied in this paper. Our numerical results support this point of view.

In the study of growth processes it is often assumed, in loose analogy with equilibrium statistical mechanics, that the fractal dimension of observed structures can be used to identify the "universality class" of the process. However, many systems out of the critical region produce space-filling aggregates. This is what one observes also in percolation for values of the density different from the critical one. Therefore, a measure of the fractal dimensions which gives the Euclidean dimension as a result may not be able to discriminate between different dynamical processes. In particular, measures of D slightly away from the critical point performed on the system described in this paper will produce values indistinguishable from 2. In this respect, the results of Ref. [9] do not discriminate between different possible growth mechanisms. If the relevance of percolation in *in vivo* blood vessel formation should be confirmed, this would be a new paradigm that should be taken into account in analyzing the scaling behavior of experimental data.

[1] B. B. Mandelbrot, *Fractal Geometry of Nature* (Freeman, New York, 1988).

[2] H. E. Stanley, *Introduction to Phase Transitions and Critical Phenomena* (Oxford University Press, New York, 1971).

[3] T. Vicsek, *Fractal Growth Phenomena* (World Scientific, Singapore, 1992).

[4] T. Vicsek, *Fluctuations and Scaling in Biology* (Oxford University Press, New York, 2001).

[5] G. B. West, J. H. Brown, and B. J. Enquist, Science **276**, 122 (1997); **284**, 1667 (1999).

[6] P. Carmeliet, Nat. Med. **6**, 389 (2000).

[7] A. Gamba, D. Ambrosi, A. Coniglio, A. de Candia, S. Di Talia, E. Giraudo, G. Serini, L. Preziosi, and F. Bussolino, Phys. Rev. Lett. **90**, 118101 (2003).

[8] G. Serini, D. Ambrosi, E. Giraudo, A. Gamba, L. Preziosi, and F. Bussolino, EMBO J. **22**, 1771 (2003).

[9] Y. Gazit, D. A. Berk, M. Leunig, L. T. Baxter, and R. K. Jain, Phys. Rev. Lett. **75**, 2428 (1995).

[10] A. C. Guyton and J. E. Hall, *Textbook of Medical Physiology*, 10th ed. (W.B. Saunders, St. Louis, MO, 2000).

[11] D. E. Ingber and J. Folkman, Cell **58**, 803 (1989).

[12] Ya. B. Zel'dovich, Astron. Astrophys. **5**, 84 (1970); S. F. Shandarin and Ya. B. Zeldovich, Rev. Mod. Phys. **61**, 185 (1989).

[13] M. Kardar, G. Parisi, and Y.-C. Zhang, Phys. Rev. Lett. **56**, 889 (1986).

[14] X. Nie, E. Ben-Naim, and S. Chen, Phys. Rev. Lett. **89**, 204301 (2002).

[15] J. Burgers, *The Non Linear Diffusion Equation* (D. Reidel, Dordrecht, 1974).

[16] E. Hopf, Commun. Pure Appl. Math. **3**, 201 (1950).

[17] J. Cole, Appl. Math. (Germany) **9**, 225 (1951).

[18] J. Bec and U. Frisch, e-print cond-mat/0012033.

[19] M. Vergassola, B. Dubrulle, U. Frisch, and A. Noullez, Astron. Astrophys. **289**, 325 (1994).

[20] J. Bec, R. Iturriaga, and K. Khanin, Phys. Rev. Lett. **89**, 024501 (2002).

[21] Y. G. Sinai, Commun. Math. Phys. **148**, 601 (1992).

[22] A. Pluen, P. A. Netti, R. K. Jain, and D. A. Berk, Biophys. J. **77**, 542 (1999).

[23] R. J. LeVeque, *Numerical Methods for Conservation Laws* (Birkhauser, Zurich, 1990).

[24] D. Stauffer and A. Aharony, *Introduction to Percolation Theory* (Taylor & Francis, London, 1994).

[25] Note that in Ref. [7] due to a misprint the threshold appears to be equal to $1/\sigma^2$.

[26] J. Hoshen and R. Kopelman, Phys. Rev. B **14**, 3438 (1976).

[27] C. Ruhrberg, H. Gerhardt, M. Golding, R. Watson, S. Ioannidou, H. Fujisawa, C. Betsholtz, and D. T. Shima, Genes Dev. **16**, 2684 (2002).